In Situ Reactivity and FTIR Study of the Wet and Dry Photooxidation of Propane on Anatase TiO2

ARTICLE *in* THE JOURNAL OF PHYSICAL CHEMISTRY B · APRIL 2005

Impact Factor: 3.3

3 AUTHORS:

Carl Hägglund
Uppsala University
37 PUBLICATIONS **921** CITATIONS
SEE PROFILE

Bengt Herbert Kasemo
Chalmers University of Technology
497 PUBLICATIONS **23,194** CITATIONS
SEE PROFILE

Lars Osterlund
Uppsala University
88 PUBLICATIONS **1,639** CITATIONS
SEE PROFILE

In Situ Reactivity and FTIR Study of the Wet and Dry Photooxidation of Propane on Anatase TiO_2

Carl Hägglund,[†] Bengt Kasemo,[†] and Lars Österlund*[,†,‡]

Department of Applied Physics, Chalmers University of Technology, SE-412 96 Göteborg, Sweden, and Department of Environment and Protection, FOI NBC Defence, SE-901 82 Umeå, Sweden

Received: December 17, 2004; In Final Form: March 14, 2005

The photocatalytic oxidation (PCO) of trace amounts of propane (500 ppm) on nanocrystalline anatase TiO_2 has been investigated in situ as a function of temperature ($T = 318-473$ K), humidity ($C_{H_2O} = 0-4\%$), and time by means of mass spectrometry and diffuse reflectance Fourier transform infrared spectroscopy (DRIFT). Propane adsorbs associatively on TiO_2 at 318 K in dry air, while at 473 K small amounts of thermal dissociation products appear on the surface. In agreement with previous studies, propane is found primarily to be converted to acetone by reactions with photogenerated oxygen radicals. Various successive reaction paths exist, where the branching depends on the temperature and hydroxylation state of the surface. Under dry conditions at 318 K, acetone oxidation is initially kinetically hindered, while, above 400 K, acetone readily decomposes. The thermally assisted reaction channel leads to detrimental bonding of surface species and inhibition of the catalytic activity. It is manifested by a coloration of the sample and suggested to be coupled to surface reduction. Under humidified conditions, there is an optimum of the PCO in C_{H_2O} and T space, which is estimated to correspond to an equilibrium coverage of one monolayer of H_2O (or bilayer). The latter reaction condition also corresponds to sustained high propane conversion and is characterized by rapid establishment of steady state rates. The optimum PCO is discussed in terms of a balance between (i) sustaining enough of a photoactive water monolayer to avoid detrimental bonding of surface species, (ii) allowing reactants to adsorb and access bulk TiO_2 photoexcitations, and at the same time (iii) maximizing the thermally assisted decomposition of intermediates.

1. Introduction

Heterogeneous photocatalytic oxidation (PCO) of organic pollutants over semiconducting metal oxides, with TiO_2 being by far the most studied example, is considered as a potentially cost-effective and efficient route for air and water cleaning.[1−3] Accordingly, there has been tremendous interest in this field, in particular during the past decade. Despite this, there are relatively few studies on PCO of simple alkanes. Most studies have dealt with the partial oxidation of alkanes because of the interest in selective alkane oxidation into fine chemicals.[4−6] The work by Teichner and co-workers in the early 1970s still serves as a reference for the overall alkane decomposition mechanism on TiO_2, namely, alkane → alcohols/alkenes → ketones and aldehydes → CO_2.[4] The detailed nature of the reaction mechanism is, however, not fully understood, and there are still discrepancies/ambiguities in the literature on the selectivity toward partial oxidation products. Moreover, very few mechanistic studies have been done to correlate surface reactions, surface species, and turnover number with possible reaction paths under different reaction conditions.[7,8]

The PCO of alkanes is reported to proceed preferentially via ketone formation through subsequent reaction with the superoxide ions or, after their recombination with a hole, with oxygen atom radicals.[4,9−11] In the case of propane, it has been reported that acetone (CH_3COCH_3) is produced as an intermediate at high C_3H_8 concentrations as well as smaller amounts of aldehydes (propanal (CH_3CH_2CHO) and ethanal (CH_3CHO)).[4,6] Photooxidation of acetone in turn has been reported to lead to formate ion (HCOO) formation.[8] Formate is frequently reported to be a stable intermediate on TiO_2,[12] and there are good reasons to believe that photooxidation of formate is a limiting step in the total oxidation of hydrocarbons on TiO_2. In general, the CO_2-to-intermediate product ratio is found to depend on the alkane/oxygen ratio in the feed. In one of these studies,[6] it was shown that the C_3H_8 conversion was highest at room temperature, where the total oxidation of C_3H_8 to CO_2 was dominant. Conversion to partial oxidation products increased as a function of temperature up to 409 K, after which it declined. Total oxidation has also been reported at low (ppm level) C_3H_8 concentrations.[13] In contrast to the PCO of C_3H_8, it has recently been shown that thermal oxidation over TiO_2 results in dehydrogenation reactions and acrolein and acetate species on the TiO_2 surface, with no detectable ketone and aldehyde partial oxidation products.[14]

In this study, we investigate in situ the PCO of C_3H_8 as a function of time and temperature in dry and humid atmospheres and determine the optimum conditions for sustained PCO of C_3H_8. With a combination of mass spectrometry (MS) and in situ diffuse reflectance FTIR spectroscopy (DRIFT), we relate surface species formed during the initial photooxidation period with the measured photocatalytic activity.

2. Experimental Section

2.1. Photocatalytic Reactor. A specially designed flow reactor with an interior volume of 6 cm^3 was employed for the photocatalytic measurements, Figure 1. The reactor was sealed on both sides with quartz windows. Samples were pressed

* Corresponding author. E-mail: lars.osterlund@foi.se.
[†] Chalmers University of Technology.
[‡] FOI NBC Defence.

10.1021/jp0442448 CCC: $30.25
Published on Web 05/04/2005

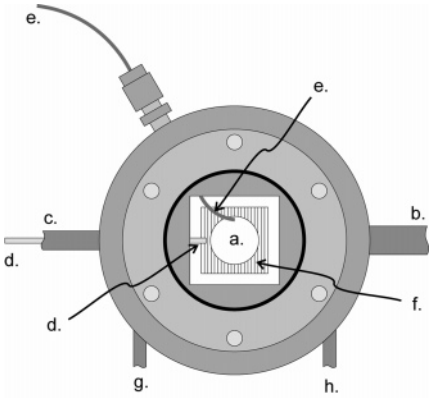

Figure 1. Schematic drawing of the photocatalytic flow reaction cell: (a) sample, (b) gas inlet, (c) gas outlet, (d) quartz capillary leak for MS, (e) thermocouple rod, (f) Kantal wire (heat source) situated behind the back window, (g) cooling water inlet; (h) cooling water outlet.

against the backside quartz glass window by a thermocouple rod, which ensured good thermal contact. Heating was provided from the backside by infrared radiation from a resistively heated Kantal wire, and the sample temperature was controlled with a PID regulator. The spatial temperature profile across the sample was uniform to within 5 K, as measured by an infrared radiation camera. During measurements, the reactor and connected gas tubing temperature was kept constant at 318 K by external heating.

Reactant gases were introduced into the cell volume through a nozzle, which distributed the gas over the entire sample. On-line mass spectrometry analysis was performed with a quadrupole mass spectrometer. An enhanced signal-to-noise ratio was achieved by minimizing the distance from the quartz capillary leak orifice to the sample and by the use of a directed-gas inlet system.[15]

2.2. Gases. High purity research gases were used as delivered without further purification. The gas flows of Ar, O_2, and 1% C_3H_8/Ar mixtures were controlled using mass flow regulators to give a 50 mL/min flow rate of the desired reactor feed mixture in the photoreactivity experiments. In the FTIR experiments, the flow rate was adjusted to 100 mL/min. The reactant gas was humidified with Milli-Q water (18.2 MΩ·cm) in a heated mixing chamber, to which the water supply was controlled by the calibrated pressure drop over a long, narrow tube.

2.3. Photocatalyst Materials. A 130 mg portion of anatase TiO_2 powder was pressed at 220 MPa into self-supporting pellets of ~1 cm^2 area. The measured BET surface areas of the pristine pellets were typically ~250 m^2/g (same as the powder). The BET area was significantly reduced to 78 m^2/g for a sample subjected to one series of reactivity measurements, indicating a surface area reduction of 69%. This area reduction was not compensated for in the analysis to obtain area-normalized PCO conversions versus time, since the detailed time dependence and mechanism of this phenomenon was not further explored. X-ray diffraction (XRD) measurements revealed a purely anatase crystal structure, both before and after the photooxidation experiments, which excludes phase transformation (anatase → rutile) as a cause for the decreased BET area. An increase of the mean particle size from about 7.0 to 10.3 nm was inferred from the XRD peak widths through the Scherrer equation, which however cannot account for the 69% BET area reduction. The pore size distribution according to the BJH method[16] was strongly shifted from a maximal incremental surface area around a pore diameter of 18 Å in the pristine TiO_2 samples to 46 Å in the sample used. The porosity was however only slightly decreased, from about 55 to 53%, which suggests that pore coalescence and TiO_2 particle growth occurred in a manner nearly conserving the total pore-to-sample volume fraction.

To recondition the samples between each PCO experiment, an oxidative sample pretreatment was applied prior to each measurement, which involved annealing the sample at 650 K for 15 min in 12% O_2 diluted in Ar (with additional water added in the humid experiments). This temperature is high enough to remove physisorbed and chemisorbed water, organic residues, as well as most acidic hydroxyl groups and organic species, but not the isolated hydroxyl groups with the highest surface binding energy.[17−19] The sample was subsequently cooled to the desired temperature in the same gas mixture. Temperature regulation allowed thermal equilibrium to be established in approximately 1 h.

2.4. Photocatalytic Reactivity Measurements. A high pressure 75 W Xe arc lamp system and additional IR- and visible-light-blocking filters provided the UV irradiation for the experiments. The irradiative power was measured ex situ in an identical optical setup using a thermopile power sensor. Unless otherwise stated, the TiO_2 sample was irradiated with a total power of 83 mW cm^{-2}, corresponding to 7.3 mW cm^{-2} UV irradiation at $\lambda < 400$ nm (1.3×10^{16} photons s^{-1} cm^{-2}). The measured photoinduced temperature change was always <4 K.

After admitting reactant gas to the reaction cell, the propane MS signal was stabilized within 15 min. Subsequently, the sample was irradiated in 5 min intervals with 5 min intermittent dark periods allowing for baseline drift to be corrected. Four periods of irradiation were used (denoted by $N = 1-4$, respectively), after which the measurement was ended with a 10 min dark period. The calculated average molecular residence time of about 7 s in the reactor compartment matched well with the measured MS response time of photoinduced reactions. Rates of removal/production were deduced from the fed/measured volume fractions C_x of reactants and products using

$$\frac{\mathrm{d}n_x(t)}{\mathrm{d}t} = \frac{PF}{RT}(C_{x,\mathrm{Meas}}(t) - C_{x,\mathrm{Feed}}) \quad (\mathrm{mol/min}) \qquad (1)$$

where P denotes the total pressure (10^5 Pa), R the molar gas constant, T the gas mixture temperature, and F the flow rate through the reactor. The volume fractions C_x were found by deconvolution of the calibrated MS cracking patterns of the introduced gas compounds. Contributions at $m/Z = 28$ were ambiguous and therefore omitted from the analysis. To account for changes in the leak rate in the quartz capillary tube due to thermal effects (such as material expansion and changes in gas viscosity and density),[20] the concentrations were in a final step normalized to yield a total sum of 100 vol % to satisfy mass balance. This was justified since the MS measurements revealed no other gas phase oxidation products ($m/Z < 60$) in addition to CO_2 and H_2O within the detection limits. The lack of additional gas phase products is consistent with the results of comparable studies using trace amounts of propane.[13]

Average rates $\bar{W}_x(N)$ for removal/production of species x ($x = C_3H_8$ or CO_2) were used to reduce the fluctuations in the data and to describe the rates not significantly affected by the rapid transients during the first minute in the PCO cycle (see Figure 2). $\bar{W}_x(N)$ is defined by the average momentary rates (eq 1) during the last minute of irradiation period N ($N = 1, 2, 3, 4$) according to

$$\bar{W}_x(N) = \overline{\frac{\mathrm{d}n_x(t_N)}{\mathrm{d}t}} \equiv \frac{1}{\Delta t}\int_{t_N}^{t_N+\Delta t}\frac{\mathrm{d}n_x(t)}{\mathrm{d}t}\,\mathrm{d}t \quad (\mathrm{mol/min}) \qquad (2)$$

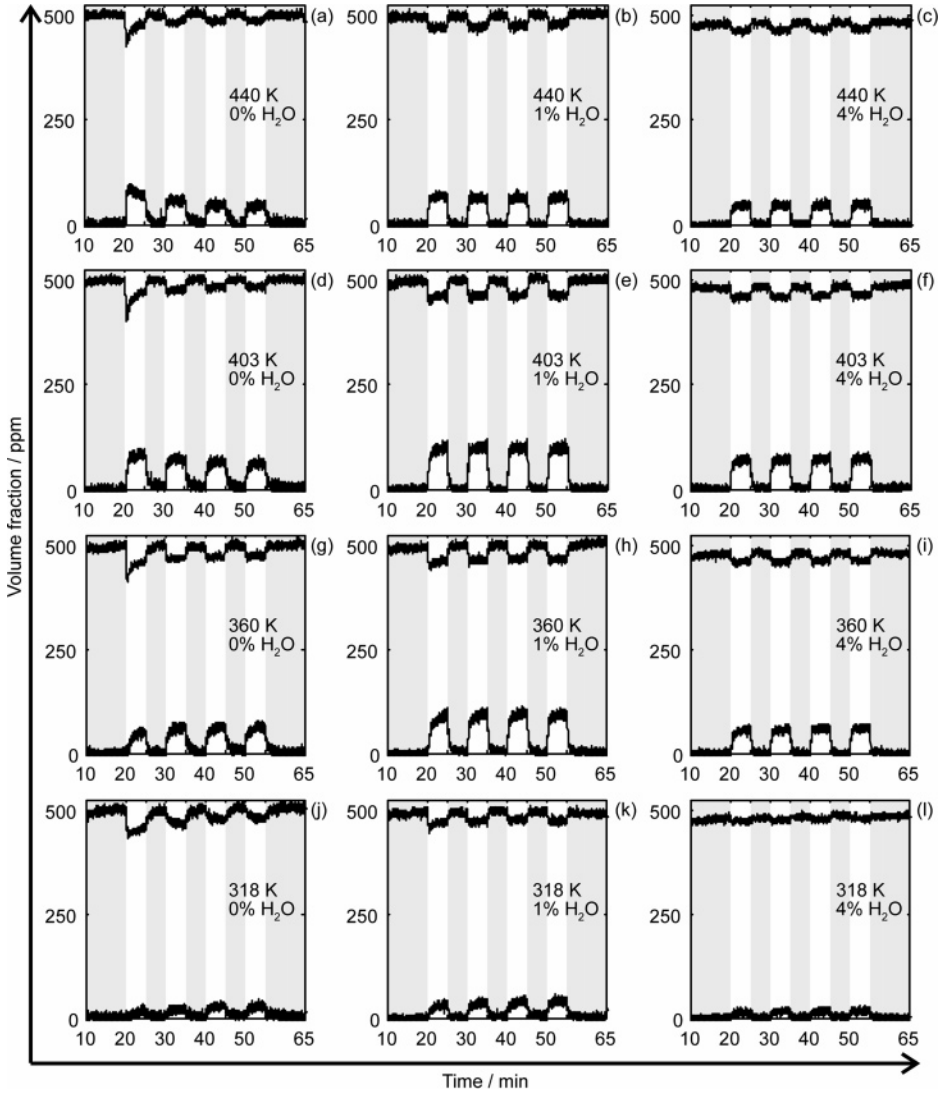

Figure 2. Mass spectroscopic signals deconvoluted into volume fractions of C_3H_8 and CO_2 as a function of time. Four periods of irradiation (in the text denoted by $N = 1-4$, respectively) each lasting 5 min are marked with white backgrounds. In each plot, the upper trace corresponds to the C_3H_8 signal and the lower to the CO_2 signal. The UV photon flux was 1.3×10^{16} photons s^{-1} cm^{-2}.

where $t_N = 14 + N \cdot 10$ min (see Figure 2) and $\Delta t = 1$ min. A repetition of the first measurement in the experimental series ($C_{H_2O} = 0$, $T = 403$ K) at the end of the whole series reproduced the reaction rates represented in this way to within 5%.

2.5. FTIR Measurements. Rapid scan diffuse reflectance FTIR (DRIFT) spectra were recorded in situ during UV irradiation using a BioRad FTS6000 spectrometer, equipped with a reaction cell mounted inside a diffuse reflectance accessory (Praying Mantis, Harrick). Pressed tablets of TiO_2 identical to those used in the photocatalysis cell were placed in a sample cup inside the DRIFT reaction cell and pretreated in the same way as in the reactivity measurements. UV irradiation was admitted through a CaF_2 window into the DRIFT cell at an angle of 45°. DRIFT spectra (2 cm^{-1} resolution) were acquired as a function of time with a time separation of 3.7 s between each spectrum. The spectra are presented as absorbance spectra calculated as $\log(1/R)$. Background spectra were collected in the dark in the reaction mixture immediately before UV light was admitted to the sample unless otherwise stated.

3. Results

The photoactivated nature of the oxidation reaction was confirmed by measurements at light intensities between 0.63 and 7.6 mW cm^{-2} equivalent UV irradiation at 403 K. Rates (both C_3H_8 adsorption and CO_2 desorption) were observed to follow irradiance to the power of 0.7 (rate $\propto I^{0.7}$). This power law dependence typically results when the e−h pair generation rate is proportional to the photon flux, but the reaction rate is suppressed by the second-order e−h pair recombination rate.[9] In contrast, ramping the sample temperature at 10 K/min in the reaction mixture up to 600 K revealed only a weak onset of CO_2 production around 480 K. Since the UV−vis irradiation-induced temperature increase was always <4 K, this observation further confirms a photoactivated reaction at all temperatures studied here. This does not exclude that intermediate reaction steps are thermally activated but shows that the initial rate-limiting step is photoactivated. The MS signals during the photocatalytic oxidation of C_3H_8 were recorded at sample temperatures from 318 to 440 K under dry conditions and at $C_{H_2O} = 1$ and 4%, respectively. Data from these measurements are shown in Figure 2. Qualitative differences are clearly observed between the dry and humid reaction conditions. Most importantly, a simultaneous maximum of $\bar{W}_{CO_2}(4)$ and $\bar{W}_{C_3H_8}(4)$ in the (C_{H_2O}, T) space around 400 K and 1% H_2O exists, meaning that the sustained $C_3H_8 \rightarrow CO_2$ conversion rate is optimum under these conditions. Further, it is seen that the C_3H_8

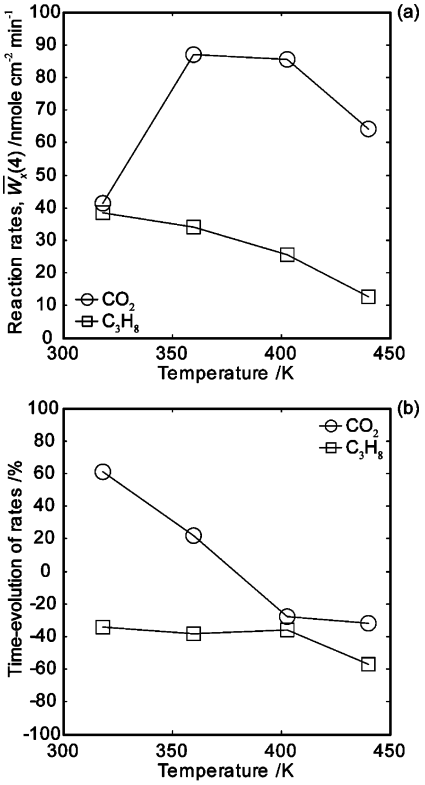

Figure 3. (a) Average photocatalytic removal and production rates $\bar{W}_x(4)$ obtained through eq 2 for $C_{H_2O} = 0\%$. (b) Time evolution of these rates compared to their values in the first irradiation interval as defined by $(\bar{W}_x(4) - \bar{W}_x(1))/\bar{W}_x(1) \times 100\%$.

removal rate is highest during the initial irradiation period under dry conditions and then falls off with time, while under humid conditions the conversion remains at a more constant level. The former is not accompanied by a corresponding CO_2 production rate, which would account for a mass balance. It is also evident from Figure 2 that irradiation memory effects on the reaction rates are notable under dry conditions but less pronounced under humid conditions. These memory effects, that is, the CO_2 "postdesorption" and C_3H_8 "postadsorption", may be ascribed to the long lifetime and reactivity of photoactivated surface centers.[21] Common for both dry and humid conditions is that the exclusion of O_2 from the reactant gas mixture results in a lack of any detectable MS response upon UV irradiation and in particular no removal of C_3H_8. The C_3H_8 adsorption is therefore concluded to involve complexation with O radicals, rendering $C_3H_6O_{(ad)}$ (adsorbed acetone, see below) and $H_2O_{(ad)}$ in agreement with previous results.[4,6] In the following, a more quantitative analysis of the data is performed.

3.1. Photooxidation in a Dry Atmosphere. The rates of C_3H_8 consumption and CO_2 production in the last irradiation interval (i.e., $\bar{W}_x(4)$ according to eq 2) are presented in Figure 3a. The C_3H_8 photoconversion rate decreases monotonically with temperature, which is tempting to assign to a diminishing C_3H_8 coverage as the gas−surface adsorption equilibrium shifts toward the gas phase with increasing sample temperature. However, the observed requirement of O_2 for net C_3H_8 adsorption to take place, the maximum in $\bar{W}_{CO_2}(4)$ and the declining C_3H_8 removal rate over time quantified in Figure 3b, implies a more complex situation. A plausible explanation is that fewer free sites are replenished for photoconversion at higher temperatures due to a site-blocking effect resulting from the accumulation of stable or slowly oxidizing species X_{stable}, whose

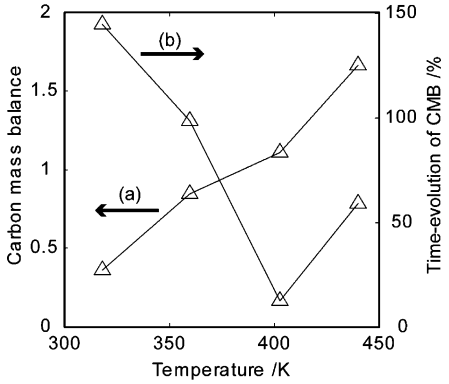

Figure 4. (a) Average carbon mass balance in Figure 2 as defined by eq 4 during the last irradiation interval under dry conditions, $\overline{CMB}(4)$. (b) The time evolution of $\overline{CMB}(N)$ in relation to its value in the first irradiation interval, $(\overline{CMB}(4) - \overline{CMB}(1))/\overline{CMB}(1) \times 100\%$. A gradual evolution of the balance toward carbon output is observed during the 20 min of irradiation at all temperatures studied.

formation is thermally assisted. Such a site-blocking mechanism has been proposed to account for similar effects in other systems before.[22]

Moreover, the accumulation of some stable carbon species falls in nicely with the observation of a clearly distinguishable, sienna brown coloration on the TiO_2 sample which, in contrast to a previous report,[13] appeared during the first few minutes of irradiation under dry conditions, especially at high temperatures. The coloration remained on the samples when flushed in a 12% O_2/Ar mixture but could, at least partially, be removed when irradiated in the same mixture. It was, however, completely removed by the pretreatment procedure described in the Experimental Section.

Finally, the site-blocking mechanism aligns with the discrepancy between the temperature dependence of the C_3H_8/CO_2 rates observed in Figure 3a, which must be ascribed to a gradual accumulation of surface species upon irradiation, since no gas phase carbon species apart from CO_2 (and C_3H_8) could be detected.

To elucidate and quantify the last point in more detail, we consider the carbon mass balance (CMB) of the total oxidation ($C_3H_8 + 5O_2 \rightarrow 3CO_2 + 4H_2O$), which implies the C_3H_8 removal rate should equal one-third of the CO_2 yield at the steady state, and compare this value to the experimentally determined CMB. Again, we distinguish between the momentary CMB and the average CMB obtained during the last minute in irradiation interval N to separate initial transients from long-term effects, namely,

$$\mathrm{CMB}(t) \equiv -\frac{1}{3}\frac{\mathrm{d}n_{CO_2}(t)}{\mathrm{d}n_{C_3H_8}} = -\frac{1}{3}\frac{\mathrm{d}n_{CO_2}(t)}{\mathrm{d}t}\Big/\frac{\mathrm{d}n_{C_3H_8}(t)}{\mathrm{d}t} \qquad (3)$$

$$\overline{\mathrm{CMB}}(N) \equiv \frac{1}{3}\frac{\bar{W}_{CO_2}(N)}{\bar{W}_{C_3H_8}(N)} \quad (N = 1, 2, 3, \text{and } 4) \qquad (4)$$

where n denotes the number of molecules according to eq 1.

The $\overline{CMB}(4)$ values shown in Figure 4a in most cases deviate from unity, indicating that the irradiation times employed here are in general insufficient to establish the full steady state conditions. This finding is rationalized by noting that the total number of C_3H_8 molecules converted during the full experimental cycles (from 20 to 60 min) shown in Figure 2 is found (through integration similar to eq 2) to be at most 8.6×10^{17}

(at 318 K). This value should be compared to the upper limit[23] of accessible, photoactive surface sites in the sample, estimated to be 1.5×10^{17} using a 5×10^{14} cm^{-2} adsorption site density,[24] 251 m^2/g specific surface area, 1.3 cm^2 projected sample area, 1 μm UV light penetration depth,[9] 55% porosity, and 3.84 g/cm^3 bulk density. Thus, at the end of the experiment, the number of adsorbed C_3H_8 molecules per photoactive site may only be of the order of one, underlining that primarily initial photooxidation processes are investigated here. It should however be emphasized that this is a lower limit to the actual turnover number due to the uncertainty associated with the number of actually photoactive sites (which can be orders of magnitude smaller) and that there may be a wide spread of turnover numbers of individual sites.[23]

Seemingly peculiar, $\overline{\mathrm{CMB}}(4)$ presented in Figure 4a goes from substoichiometric values (<1) at low temperature to "superstoichiometric" values (>1) at high temperature and breaks even around 380 K. Not only is $\overline{\mathrm{CMB}}(4)$ "too" high, but it also displays an increasing trend at 440 K (see Figure 4b). The explanation is that the net rates of C_3H_8 consumption and CO_2 production are both decreasing with time at high temperature (Figure 3b) and that the C_3H_8 adsorption rate is decreasing disproportionally faster. Through photoinduced fragmentation of C_3H_8 at the surface, an occupation (by C_1 and/or C_2 species) of up to three adsorption sites per molecule is possible. Relating to the previous discussion of stable surface species X_{stable} accumulating at high temperatures, some of the sites may be blocked for readsorption of C_3H_8 for a long time, leading to the decreasing trends with both time and temperature. However, the disproportionality of the decrease with time indicates that some CO_2 is released to the gas phase in the site-blocking process, either during the formation of X_{stable} or by degradation within the experimental time of some byproducts to X_{stable}. Thus, the path leading to site blocking can be summarized as

$$C_3H_xO_{y(\mathrm{ad})} + \alpha O_2 \xrightarrow{\mathrm{heat}(+h\nu)} \beta X_{\mathrm{stable(ad)}} + \chi CO_{2(\mathrm{ad})} + \delta OH/H_2O_{(\mathrm{ad})} \quad \text{(R1)}$$

where $1 \le \beta \le 2$, $1 \le \chi \le 2$, and $\delta \ge 0$. This does not exclude that the thermally assisted formation of X_{stable} is paralleled by alternative reaction paths and can eventually be considered a sidetrack to a more sustainable route for PCO dominating under more favorable conditions, as further articulated below.

At low temperature, Figure 4b illustrates an even stronger shift of the CMB toward CO_2 output over the experimental time (by almost 150% at 318 K). However, in contrast to at high temperature, the CO_2 production rate (Figure 3b) increases toward the stoichiometric value and continues to do so even during an extended period of irradiation over a total of 60 min (not shown). Together with the observation that the integrated, total C_3H_8 adsorption is more than a factor of 2 higher at 318 than at 440 K, the conclusion is that the surface carbon accumulation is very high but predominantly in a form that does not appreciably block sites for further C_3H_8 adsorption. Very weak coloration of the sample is observed, even after extended irradiation time. A branching mechanism is therefore proposed, where some *photoactivated* event promotes a reaction path other than the *thermally* assisted formation of X_{stable}. While the photoactivated event occurs at a virtually unreduced pace at low temperature, thermally activated steps are obviously slow, which shifts the branching ratio toward the other, more sustainable reaction. In the following, we investigate if the formation of adsorbed H_2O or OH species in conjunction with the C_3H_8 adsorption and intermediate formation constitutes such an event.

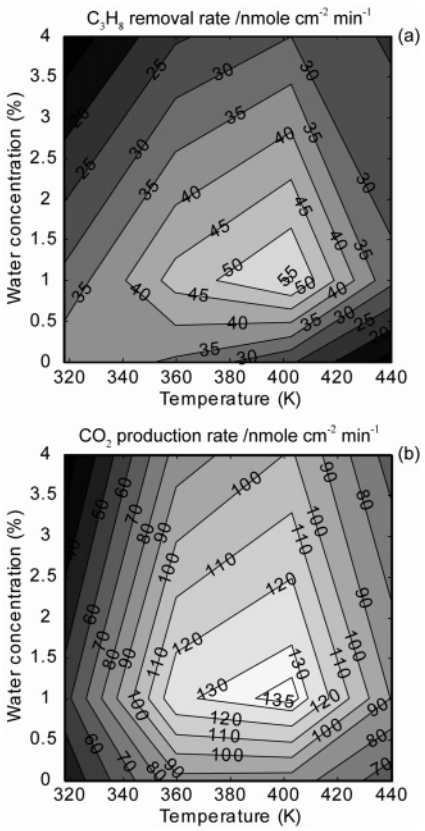

Figure 5. Contour plots of (a) the final removal rate $\bar{W}_{C_3H_8}(4)$ of C_3H_8 and (b) the final production rate $\bar{W}_{CO_2}(4)$ of CO_2 (see eq 2). Peak values of 56 and 138 nmol cm^{-2} min^{-1} are found for C_3H_8 and CO_2, respectively, at 403 K and 1% H_2O.

3.2. Photooxidation in a Humid Atmosphere. Due to the production of H_2O in the PCO reaction, addition of some H_2O to the reaction mixture should be expected to bring the system closer to steady state conditions. Measurements in humid atmospheres are shown in the middle and right columns of Figure 2. The results of the reaction rates are shown in Figures 5−7 and are presented in a similar manner as for the dry case (cf. Figures 3 and 4) but as contour plots in order to capture the entire parameter space.

In general, no mass spectroscopic evidence of a photoinduced gas phase change of the H_2O concentration was detected. Only at the highest relative humidity (at 318 K and 4 vol % H_2O), when adsorbing surfaces (reactor walls, etc.) are practically saturated with H_2O, were distinct concentration changes observed that correlated with the irradiation intervals. When the humidity was gradually increased during or after irradiation, a large amount of desorbing CO_2 was detected. Displacement of CO_2 by H_2O has been previously observed on TiO_2.[8]

It is apparent from Figure 2 that the presence of H_2O influences the PCO reaction considerably and that the concentration of H_2O is a candidate control parameter for the proposed branching mechanism. The transient behavior observed under dry conditions is essentially damped, and much less brown-yellow coloration appears on the sample. Figure 5 further shows that the $\bar{W}_x(4)$ rates (for both C_3H_8 and CO_2) peak simultaneously at 1% H_2O concentration and 403 K. The corresponding quantum yields, defined as the number of converted molecules per incident UV photon (λ < 400 nm), are 4.2 and 10.6% for

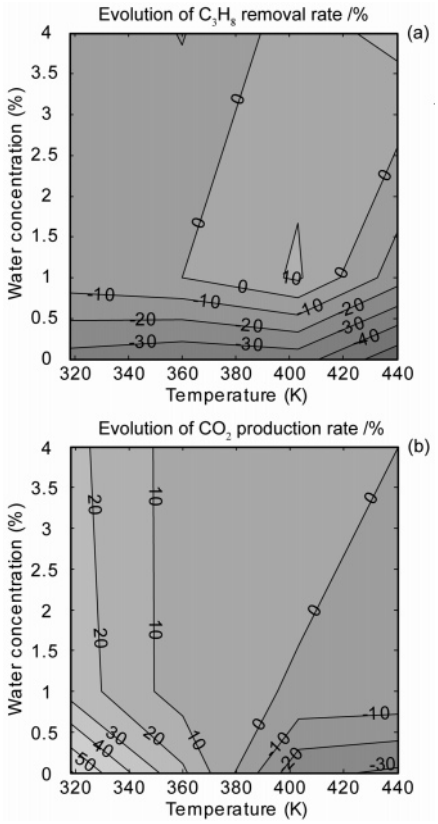

Figure 6. (a) Contour plots of the relative change over time of the average C_3H_8 removal rate in the last irradiation interval compared to the first using eq 2 as $(\bar{W}_{C_3H_8}(4) - \bar{W}_{C_3H_8}(1))/\bar{W}_{C_3H_8}(1) \times 100\%$. (b) Analogous for the CO_2 evolution.

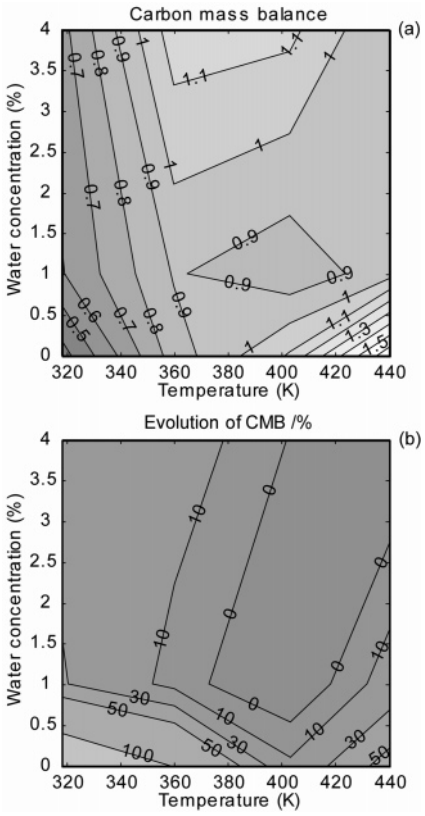

Figure 7. Contour plots of (a) the carbon mass balance (eq 3) during the last irradiation interval in Figure 2. A value of 1 corresponds to stoichiometric production (and desorption) of CO_2. (b) Time evolution of the carbon mass balance, $(\overline{CMB}(4) - \overline{CMB}(1))/\overline{CMB}(1) \times 100\%$.

C_3H_8 and CO_2, respectively. This underscores the beneficial role of H_2O and the complex dependence on temperature and humidity.

Simultaneously, the photoresponse at 403 K, without any O_2 in the gas feed mixture but with high water concentrations (near saturation), results in no measurable C_3H_8 conversion rate and no noticeable coloration of the TiO_2. Thus, as already stated, H_2O is not able to initiate the PCO reaction alone. Rather, the transient C_3H_8 adsorption is damped, and the main, long-term beneficial role of H_2O ought to be ascribed to a subsequent reaction step, such as in promoting the proposed more sustainable branch for the decomposition of the primary intermediate (which is identified as acetone in section 3.3).

It should further be noted that the effect of H_2O is not only positive and that the PCO rate deteriorates at too high concentrations, as seen in Figure 5. This, as well as the decreasing $W_{C_3H_8}$ trend observed with time at low temperature in the dry case, can be ascribed to competitive adsorption between reactants and H_2O, as will be further discussed. In contrast to the dry case, the C_3H_8 removal rate is accordingly quite constant with time in humid atmospheres, and especially so in the temperature range from 380 to 420 K, Figure 6a. The CO_2 production rate increased with time under all but the dry conditions for $T > 390$ K but was also much stabilized with increasing H_2O feed, Figure 6b.

Since the enthalpy of water adsorption on TiO_2 is reported to be 12.2 kcal/mol[25] and the sublimation energy of condensed water (multilayer) is 10.4 kcal/mol, it is possible to make an estimate of the expected range of the water coverage on the surface at 380 K and 1% H_2O in the feed (which we interpolate to be the optimum reaction condition). Assuming nonactivated adsorption with unit sticking probability and a tight transition state (normal pre-exponential factor 10^{13} s^{-1}), we calculate a coverage between 0.3 and 3 ML, where 1 ML is defined as a bilayer of water molecules (1.15×10^{15} molecules/cm^2).

Addition of $\geq 1\%$ H_2O produces an almost stoichiometric CO_2 output above 360 K (Figure 7a), which together with the high, stable rates indicates that the reaction proceeds close to the steady state in this region during the final irradiation period. From Figure 7b, it is interesting to note that the steady state conditions are reached most rapidly under conditions similar to those at which the $C_3H_8 \rightarrow CO_2$ conversion is the most efficient (403 K, 1% H_2O). Thus, the condition realizing a long-term maximum PCO rate appears to manifest already at an early stage as a minimized settling time toward the asymptotic rate.

3.3. Diffuse Reflectance Spectroscopy. To investigate further the surface species involved in the PCO, DRIFT spectra were recorded under dry conditions at 318, 403, 440, and 473 K. The background DRIFT spectra of the irradiated TiO_2 sample were collected in the reaction mixture immediately before the UV light exposure. To explicitly detect the evolution of the dark (thermal) reactions prior to irradiation, spectra were also recorded after 10 min at the desired temperature, which in turn were referenced to background spectra obtained after 1 and 5 min, respectively, after the gas mixture was admitted to the DRIFT cell. Apart from variations of feed concentrations (partly due to surface reactions), the gas phase and TiO_2 substrate contribution can therefore to some extent be eliminated from the spectra. Large fluctuations were observed in the 1700−1500 cm^{-1} range associated partly with H_2O, which prevented a detailed functional group analysis. This is (slightly less) evident also in the ν(O−H) region at 3600−3700 cm^{-1}. We will therefore in the following focus on the ν(C−H) and ν(O−H)

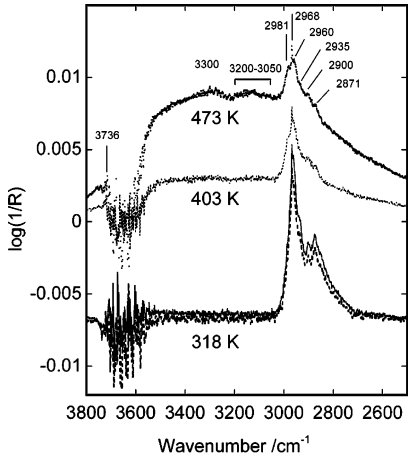

Figure 8. DRIFT spectra obtained under dry conditions in the dark at the indicated temperatures with a feed of 500 ppm C_3H_8. The DRIFT background spectrum was obtained immediately after introduction of the reactive gas mixure and in one case (at 318 K) also after 5 min of reactant exposure (dashed line). They show the primary contributions of thermal reactions to the spectra in Figure 8.

stretching regions, a restriction which prevents an unambiguous determination of surface intermediates.

Figure 8 shows DRIFT spectra obtained in the dark in the reaction mixture. Clearly resolvable ν(C−H) absorption bands are observed at 2968, 2900, and 2871 cm^{-1} at 318 K. The frequencies of these bands are very close to gas phase C_3H_8,[26] irrespective of the background spectra used (1 or 5 min in the feed), and suggest a dominant contribution of gas phase (like) species, which indicates mainly physisorbed C_3H_8. At $T > 400$ K, the intensity of the ν(C−H) bands decreases and a shoulder develops at 2981 cm^{-1}, in fair agreement with the $\nu_a(CH_3)$ mode in acetone on anatase TiO_2, which is expected to form under these conditions.[8,14,27] This occurs simultaneously as water absorption bands at 3200−3550 cm^{-1} evolve, indicating rearrangement of H_2O around the thermally formed surface species. At 473 K, a broad band appears in the 3050−3200 cm^{-1} region. In analogy with previous studies, this may be indicative of a thermal dehydrogenation reaction taking place at elevated temperatures.[14] Together with the observed onset of CO_2 desorption around 480 K during temperature ramp MS measurements, the DRIFT spectra in the dark thus support a weak, thermally activated partial oxidation channel in the interval 400 K < T < 480 K.

As previously reported,[8,19,28,29] infrared spectra of native TiO_2 display a broad absorption band extending from 2400 to 3900 cm^{-1}, due to collective and molecular TiO−H stretching vibrations in different local environments. No pronounced changes occur upon heating in inert gas between 318 and 473 K, implying that these OH groups are stable up to at least 473 K. Upon UV irradiation, the surface reflectivity decreases due to absorption by mobile charge carriers,[19] and a continuous upshift of the baseline of the DRIFT spectra is observed in Figure 9. A broad absorption band evolves at ≈3686 cm^{-1} upon UV irradiation, which is absent at higher temperatures ($T >$ 400 K) and bleached in the dark in an O_2 atmosphere. This band is attributed to OH radicals coordinated to Ti(IV) sites in agreement with previous studies.[19]

A narrow band develops at 3736 cm^{-1} upon UV irradiation and rapidly decreases as a function of irradiation time in the reaction mixture, see Figure 9. The half-width and position of the peak remain constant as a function of time at all temperatures and suggest that it is associated with an isolated OH group.

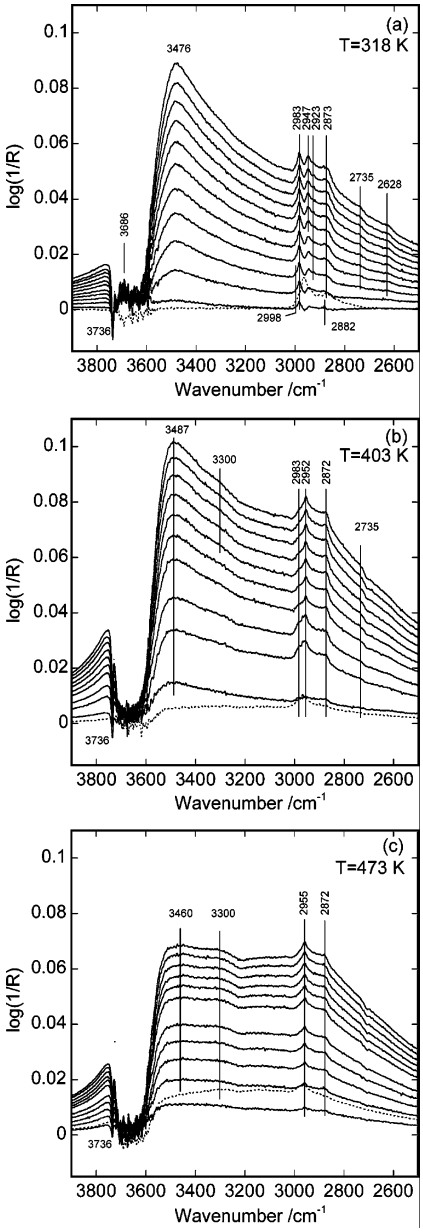

Figure 9. DRIFT spectra recorded during UV irradiation under dry conditions in the reaction mixture (100 mL/min) at (a) 318 K, (b) 403 K, and (c) 473 K, respectively. The background DRIFT spectrum (dashed lines) was obtained in the dark immediately before UV irradiation (in the reaction mixture). The spectra shown were recorded sequentially after 1 min (bottom spectrum) to 15 min (top spectrum) after the beginning of the UV irradiation.

The 3736 cm^{-1} peak lies in the upper region reported for isolated OH groups on anatase TiO_2[18,30,31] (cf. 3738 cm^{-1} in gas phase OH radicals[26]). It has been reported that a band due to Si impurities occurs around 3730−3740 cm^{-1}.[26,30,32,33] In separate X-ray photoelectron spectroscopy measurements, we could, however, not detect any Si but contain according to the manufacturer 280−300 mg of SiO_2/kg, equivalent to an Si impurity concentration around 140 ppm. We therefore tentatively assign the band at 3736 cm^{-1} to isolated OH groups coordinated with Si impurities. The removal of the isolated OH groups at 3736 cm^{-1} under dry conditions occurs on a similar time scale at all temperatures as the decay of the initial C_3H_8 removal rate, which rules out thermally activated processes. One scenario considered is therefore that the initially produced H_2O leads to hydrogen bonding between the isolated Si−OH groups syn-

chronously with the C_3H_8 removal, thereby shifting the 3736 cm^{-1} peak into the broad peak associated with OH/H_2O networks. However, since no other consistent frequency changes are detected in the ν(O−H) region, a link to the initial C_3H_8 behavior may alternatively be a photoreaction of isolated SiOH groups with C_3H_8 or acetone. This would point to an interesting synergetic effect between TiO_2 and Si and suggest a way to manipulate the activity of TiO_2.

During irradiation at 318 K, the 3476 cm^{-1} band intensity immediately increases due to H_2O formation. After 15 min of irradiation at 403 K, this band is shifted to 3487 cm^{-1} and at the same time a new broad band appears centered at ≈3300 cm^{-1}. The latter peak can also be discerned after thermal annealing for 15 min at 473 K. In agreement with other studies, these findings suggest that we have two types of OH stretching vibrations originating from molecular water in different local environments.[30] One type is a "liquid" state, which initially shifts to higher frequency as water desorbs and the hydrogen-bonded network is disrupted. A second type is associated with the peak around 3300 cm^{-1}, which is a result of rearrangement of the H_2O molecules and is associated with molecular water coordinated to surface species formed in the course of the PCO reaction (or thermal reaction at higher temperatures).

From Figure 9, it is evident that three strong and two weak absorption bands appear after UV irradiation in the ν(C−H) stretching region at 2800−3000 cm^{-1}. The spectra obtained at 318 K differ qualitatively from those obtained above 400 K. At 318 K, a large peak at 2983 cm^{-1} with a small shoulder at 2998 cm^{-1} and a distinct peak at 2882 cm^{-1} appears immediately upon UV irradiation. This can be assigned to acetone formation.[4,6,8] The 2998 and 2882 cm^{-1} bands are clearly discernible only during the first 1 min irradiation period. Simultaneously, the 2964 cm^{-1} peak, apparent in Figure 8 (associative adsorption in the dark), disappears (depicted by the negative band at 2964 cm^{-1}). After a time lag of 45 s, bands at 2882 and 2943 cm^{-1} develop, which shift to 2872 and 2947 cm^{-1}, respectively, after 15 min of UV irradiation.

In contrast, at $T > 400$ K, only two strong absorption bands appear at 2952 and 2872 cm^{-1}, immediately upon irradiation. The 2983 cm^{-1} peak, apparent at 318 K, is only visible initially at 403 K but gradually disappears during the 15 min of UV irradiation time (Figure 9). Similarly, the 2923 cm^{-1} peak is not clearly resolvable at $T > 400$ K. The latter indicates that, at high temperatures or after extended UV irradiation, rather stable surface species associated with the 2953 and 2872 cm^{-1} bands build up during the irradiation time. Guided by previous studies, these bands are attributed to coordinated formate species.[8,34−36] A clue to a plausible photoinduced reaction sequence comes from the observation that, as the 2998 and 2882 cm^{-1} peaks disappear as a function of irradiation time at 318 K, broad absorption bands at 2735 and 2628 cm^{-1} appear, where the latter is absent at $T > 400$ K. The former lies in the region typical for aldehydes, ν(HCO),[37] while the latter may be associated with species derived from carboxylates, such as acetate ions.[26,36]

4. Discussion

In the following, we focus on the observed difference of the photocatalytic activity under dry and wet conditions and discuss the initial versus sustained reaction mechanisms. We begin by discussing the surface hydroxylation and possible sources of photoinduced radicals, since this has direct impact on the observed kinetics. It is widely accepted that OH ions derived from water can trap holes to produce OH radicals with strong oxidizing power.[9,28]

$$\text{exciton } (h^+ - e^-) + OH^- \rightarrow OH^\bullet + e^- \qquad \text{(R2)}$$

On a water-free and fairly dehydroxylated surface, which is the case initially here after our pretreatment procedure under dry conditions, reaction via hole oxidation may also be expected to be of some importance, namely,

$$h^+ + HC \rightarrow HC^+ \qquad \text{(R3)}$$

After our pretreatment at 650 K in 12% O_2, only the most strongly held OH groups remain on the surface, while hydrogen bonded and acidic OH groups as well as molecular H_2O are removed.[17,30,38,39] The available paths to trap photoholes in the above reaction scheme are therefore through tightly bonded OH groups (R2) or C_3H_8 (R3). Without efficient repopulation of the OH groups, reaction R3 would become increasingly important after an initial reaction period. Conversely, production of H_2O/OH in the reaction shifts the balance toward the OH mediated reaction R2.

It has been shown that the presence of OH groups on the surface is greatly beneficial for the photoactivated adsorption of O_2.[40] Simultaneously, O_2 is essential for a high catalytic activity,[22,41] as clearly observed in this work. This underscores the intimate coupling of charge separation (avoiding direct electron−hole pair recombination) on one hand and oxygen and hydroxyl radical formation on the other.

It is well accepted that adsorbed O_2 is an efficient electron acceptor, forming O_2^- and O^- species.[9,38,42] On a molecular level, we may distinguish between the action of Ti(III) and Ti(IV) sites, namely,[43]

$$e^- + Ti^{4+} \rightarrow Ti^{3+} \qquad \text{(R4)}$$

$$Ti^{3+} + O_{2(ad)} \rightarrow Ti^{4+} + O_{2(ad)}{}^- \qquad \text{(R5)}$$

Since the O vacancies are reduced in number after our preparation procedure,[44] it is likely that photoadsorption of O_2 occurs mainly through reaction R5 rather than via dissociative O_2 adsorption at O vacancies. Reaction R5 requires that the surface Ti atoms become reduced (R4), which could also be realized by (reaction-induced) lattice O removal[19,41] or the presence of defect sites (which exposes trivalent Ti atoms). However, it has been reported that the presence of Ti(III) should show up as an absorption band at 3716 cm^{-1} originating from $Ti(III)O-H^-$ species.[19] The results in Figure 9 provide only conclusive support for the presence of OH radicals bonded to Ti(IV) sites and, since O_2 is a prerequisite for the PCO in this study, lead us to suggest that the initial radical formation is dictated by reactions R4 and R5, involving direct electron transfer to adsorbed O_2, resulting in a valence band hole and oxygen radical species. This then leads to the anticipated acetone and H_2O formation, as schematically depicted in Figure 10.

The acetone formation, as discussed and in agreement with previous findings,[4,6] is supported by the 2983 cm^{-1} peak in the dry-case DRIFT data (Figure 9), which suggests further that acetone forms readily at low temperatures and decomposes rapidly at higher temperatures. The transient formation of the 2998 and 2882 cm^{-1} bands suggests a similar scenario for the C_2 species (such as acetate),[36] albeit thermally less stable. The observation that CO_2 production is thermally assisted, combined with the temperature dependence of the peaks associated with C_3 and C_2 intermediates (2983 and 2998 cm^{-1}), suggests that PCO of acetone is limiting at low temperature.

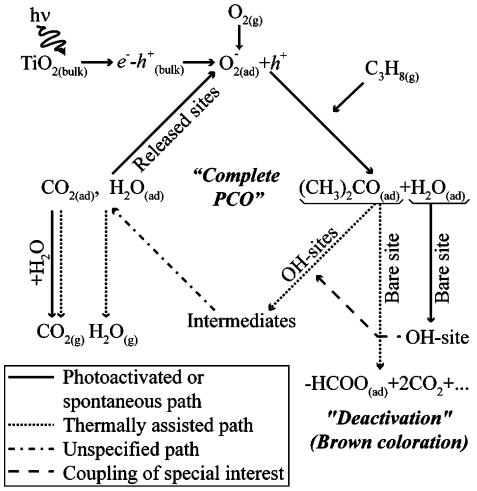

Figure 10. Important reaction paths in the photooxidation of propane. The primary intermediate is identified here with acetone ($(CH_3)_2CO$)), whereas the stable surface species X_{stable} in R1 is suggested to be mainly formate ($-HCOO$) chemisorbed to bare, exposed lattice sites, causing partial deactivation. Hydroxylated sites provide a more efficient route and lead to complete and sustained photocatalytic oxidation. Temperature and humidity control the branching, which is also affected by the H_2O produced in the photoreactions.

At all temperatures, strong bands evolve around 2950 and 2870 cm^{-1} (it shifts from 2947 to 2953 cm^{-1} at low temperatures) at the same time as the other ν(C−H) peaks gradually disappear, which is attributed to bridge-bonded (or bidentate) formate species.[8,34−36] In particular, it was previously reported (at 298 K) that formate is an intermediate to the PCO of acetone under both dry and humid conditions.[8] Formate is a thermally stable surface species which gradually accumulates during the PCO reaction. Our findings show that these (formate) species do not desorb at $T < 473$ K and may thus account for deactivation through blocking of subsequent O_2 and/or C_3H_8 adsorption. At $T > 400$ K, under the dry conditions, adsorbed C_3H_8 is readily transformed into formate by UV irradiation, as evidenced by the disappearance of the 2983, 2998, and 2923 cm^{-1} peaks and the replacement of the broad bands at 2735 and 2628 cm^{-1} by an intense low frequency tail of the 2872 cm^{-1} peak. This can be interpreted as a rapid oxidation of acetone, aldehyde, and carboxylate species at elevated temperatures, supporting the anticipated thermal assistance of CO_2 production. The concomitant temperature dependence of water formation (cf. the broad and rapidly growing peak centered at 3476 cm^{-1} in Figure 9a) supports this reaction scheme. The reactions involve a number of intermediate steps (e.g., reaction of acetone with the photoproduced radicals O_2^- and $OH^\bullet$, and possibly also $CO_{2,ad}$[8]). Without UV irradiation, a broad absorption band appeared in the 3050−3200 cm^{-1} region (Figure 8). These bands are not observed in the course of the PCO reaction, which shows that the partial oxidation reaction path is different from the PCO. We can thus summarize our findings as (see also Figure 10) the following:

$$C_3H_{8(g)} + O_{2(g)} \xrightarrow{TiO_2+h\nu} C_3H_8 - O_{2(ad)}{}^- + h^+ \xrightarrow{TiO_2+h\nu} (CH_3)_2CO_{(ad)} + H_2O_{(ad)} \xrightarrow{T+h\nu} HCOO_{(ad)} + ... \xrightarrow{T(+h\nu)} CO_2 + H_2O \quad \text{(R6)}$$

where formate (HCOO) is identified with X_{stable} in reaction R1. It is clear that the HCOO formation is related to the presence of exposed Ti sites and/or deprotonated O sites (lattice O) resulting from the pretreatment. If formate coordination to the surface is prevented by hydroxylation, the coupling to the supply of H_2O immediately follows. To justify the brown coloration, the complex bonding is believed to be associated with electron donation and reduction of the TiO_2 lattice, possibly leading to complete lattice O abstraction which is a condition well-known to be manifested by such effects.[45]

Finally, we discuss the finding of the observed optimum of the sustained PCO in the temperature−humidity parameter space. The role of water has been an issue of controversy in the photocatalysis community, where both inhibited[2] and improved[8,46] PCO has been reported. Our reactivity measurements, as well as other studies,[8] demonstrate that the CO_2 production rate is much facilitated on a hydrated surface. This supports the complete PCO route outlined in Figure 10 where acetone oxidation is enhanced by the hydroxylated sites, whereas sites are gradually deactivated in the hot, dry case. The H_2O photoproduced in concert with the acetone formation emerges as an important source of hydroxylated sites at low temperature (when the thermally activated processes are slowed compared to the photoactivated ones), shifting the balance away from the deactivating reaction and toward the complete PCO. This branching mechanism leads to a low degree of coloration (and deactivation) at low temperature, despite the highest accumulation of intermediates (e.g., acetone) on the surface, as evidenced by the very low and only slowly increasing CMB. Thus, at low temperature, acetone decomposition is rate determining and results only to a low degree in the formation of stable species, such as formate. On the other hand, at elevated temperature, the surface is maintained more dehydroxylated and coordination of stable species results in transient inhibition of the PCO and surface reduction. An induced shift in the branching imposed by the production of water in the PCO itself may eventually put a limit to the deactivation also at high temperature.

The role of H_2O may be better recognized by consideration of the qualitatively different surface conditions resulting from the different water concentrations and temperatures investigated. Under relatively dry and hot conditions, bare, undercoordinated Ti (e.g., Ti^{3+} sites) and O ions are initially exposed to the gas phase. Here, it is vital that the rate of hydroxyl supply is high enough to avoid thecoordination of stable surface species and subsequent surface reduction. At low temperature in Figure 9, it is seen that Ti(IV)−$OH^\bullet$ species are present (Figure 9a) under dry conditions, whereas these exhaust at $T > 400$ K. The latter is concerted by a buildup of formate and coloration of the surface. Once a small amount of water is supplied as byproducts from the PCO or by other means, a mixed monolayer of H_2O and OH groups forms and terminates the TiO_2 surface,[44,47] continually reoxidizing the surface[48] and continually supplying OH for the reaction. At higher water concentrations, water physisorbs on top of this monolayer. The reactivity measurements show that sustaining on the order of one monolayer of water on the surface is crucial to protect it from detrimental bonding with carbon species and associated deactivation (section 3.2). The maximum in the photoyield is then a compromise between the thermal assistance of surface reactions and the maintenance of a sufficiently hydrated/hydroxylated surface, where photoexcited e−h pairs interact with HC primarily via the H_2O/OH layer (R2) rather than at exposed lattice sites (R3). This scenario is consistent with recent results based on ^1H NMR spectroscopy.[47] It follows also from this argument that too high humidity and physisorbed water is also undesirable (as seen in Figure 2), due to diminished accessibility between the TiO_2 band

gap excited charge carriers on one hand and the reactants supplied from the gas phase on the other.[9,47]

In light of the proposed scheme, the observation that the optimum temperature and humidity are those for which the steady state is the most rapidly established is not too surprising. A minimum accumulation of intermediates at the steady state plausibly corresponds to the most rapid steady state establishment in the temperature−humidity parameter space, since this deviates the least from the initial condition of the surface. The accumulation of intermediates is proportional to the C_3H_8 adsorption rate but negatively proportional to the CO_2 production rate. According to the proposed reaction scheme (Figure 10), the C_3H_8 adsorption rate is controlled primarily by the photon flux, which is constant, whereas the CO_2 production rate is in a more direct manner related to humidity and temperature. The peak in CO_2 production (which imposes a peak in the long-term C_3H_8 adsorption rate through secondary effects) therefore implies a minimized amount of surface intermediates at the steady state.

5. Conclusions

We have shown that small amounts of propane (500 ppm) in oxygen (12%) are photocatalytically oxidized to CO_2 and H_2O on anatase TiO_2 by a mechanism where both oxygen and adsorbed water play crucial roles at different stages of the reaction, which leads to a complicated dependence on temperature and humidity. The data cohere qualitatively to a reaction scheme where C_3H_8 is initially oxidized into acetone through reaction with photogenerated oxygen radicals and direct hole pairing. Under dry conditions, acetone decomposes via thermally assisted intermediate steps, leading partially to the formation of (at least one) stable surface species (bridge-bonded formate), which binds strongly to exposed Ti sites. The stable intermediates inhibit the catalytic activity and may be associated with TiO_2 reduction, which is well-known to lead to coloration. A small amount of added water (and to some extent reaction produced water) avoids deactivation of TiO_2 and maximizes the sustained photocatalytic oxidation of C_3H_8. It also prevents the coloration of the sample. This is due to a favorable hydration of the surface and a continuous supply of hydroxyl radicals, which suppresses alternative pathways such as reactions with lattice O or Ti and prevents the formation of stable carbon species on the surface. Water also helps displace CO_2 from the surface. The conditions realizing the maximum sustained rates are found at 403 K with 1% water in the feed, and they result as a balance between the maintenance of a rapid thermally assisted decomposition of C_3 (acetone) and C_2 (e.g., acetate) intermediates while at the same time sustaining the photoactive water monolayer and avoiding the reactions leading to site blocking. These conditions coincide well with those minimizing the time for the steady state to establish at our particular UV photon flux, which is plausibly connected to a minimized net accumulation of intermediates on the surface upon irradiation.

Acknowledgment. Assistance by Martin Andersson at the Department of Applied Surface Chemistry, Chalmers University of Technology, is gratefully acknowledged for XRD, BET, and porosity measurements of the TiO_2 samples.

References and Notes

(1) Fujishima, A.; Hashimoto, K.; Watanabe, T. *TiO_2 Photocatalysis. Fundamentals and Applications*; BKC, Inc.: Tokyo, 1999.

(2) *Photocatalytic Purification and Treatment of Water and Air*; Ollis, D. F., Al-Ekabi, H., Eds.; Elsevier: Amsterdam, The Netherlands, 1993.

(3) Hoffmann, M. R.; Martin, S. T.; Choi, W.; Bahnemann, D. W. *Chem. Rev.* **1995**, *95*, 69.

(4) Djeghri, N.; Formenti, M.; Juillet, F.; Teichner, S. J. *Faraday Discuss. Chem. Soc.* **1974**, *58*, 185.

(5) Pitchai, P.; Klier, K. *Catal. Rev.—Sci. Eng.* **1986**, *28*, 13.

(6) Wada, K.; Yoshida, K.; Takatani, T.; Watanabe, Y. *Appl. Catal., A* **1993**, *99*, 21.

(7) Martra, G.; Coloccia, S.; Marchese, L.; Augugliaro, V.; Loddo, V.; Palmisano, L.; Schiavello, M. *Catal. Today* **1999**, *53*, 695.

(8) El-Maazawi, M.; Finken, A. N.; Nair, A. B.; Grassian, V. H. *J. Catal.* **2000**, *191*, 138.

(9) Peral, J.; Ollis, D. F. *J. Catal.* **1992**, *136*, 554.

(10) Fujishima, A.; Rao, T. N.; Tryk, D. A. *J. Photochem. Photobiol., C* **2000**, *1*, 1.

(11) Sinev, M. Y. *J. Catal.* **2003**, *216*, 468.

(12) Diebold, U. *Surf. Sci. Rep.* **2003**, *48*, 53.

(13) Brigden, C. T.; Poulston, S.; Twigg, M. V.; Walker, A. P.; Wilkins, A. J. J. *Appl. Catal., B* **2001**, *32*, 63.

(14) Hasan, M. A.; Zaki, M. I.; Pasupulety, L. *J. Phys. Chem. B* **2002**, *106*, 12747.

(15) Hall, J.; Lundgren, S.; Keck, K. E.; Kasemo, B. *Int. J. Mass Spectrom. Ion Processes* **1991**, *108*, 1.

(16) Barret, E. P.; Joyner, L. G.; Halenda, P. P. *J. Am. Chem. Soc.* **1951**, *73*, 373.

(17) Misra, D. N. *Nature (London), Phys. Sci.* **1972**, *240*, 14.

(18) Primet, M.; Pichat, P.; Mathieu, M.-V. *J. Phys. Chem.* **1971**, *75*, 1216.

(19) Szczepankiewicz, S. H.; Colussi, A. J.; Hoffmann, M. R. *J. Phys. Chem. B* **2000**, *104*, 9842.

(20) Lundgren, S.; Keck, K.-E.; Kasemo, B. *Rev. Sci. Instrum.* **1994**, *65*, 2696.

(21) Polikhova, S. A.; Andreev, N. S.; Emeline, A. V.; Ryabchuk, V. K.; Serpone, N. *J. Phys. Chem. B* **2004**, *108*, 2354.

(22) Peral, J.; Domenech, X.; Ollis, D. F. *J. Chem. Technol. Biotechnol.* **1997**, *70*, 117.

(23) Serpone, N.; Emeline, A. V. *Int. J. Photoenergy* **2002**, *4*, 91.

(24) Childs, L. P.; Ollis, D. F. *J. Catal.* **1980**, *66*, 383.

(25) Raupp, G. B.; Dumesic, J. A. *J. Phys. Chem.* **1985**, *89*, 5240.

(26) NIST Mass Spec Data Center; Stein, S. E. (director). Infrared Spectra. In *NIST Chemistry WebBook, NIST Standard Reference Database Number 69*; Mallard, W. G., Ed.; National Institute of Standards and Technology: Gaithersburg, MD, March 2003.

(27) Zaki, M. I.; Hasan, M. A.; Pasupulety, L. *Langmuir* **2001**, *17*, 768.

(28) Munuera, G.; Rives-Arnau, V.; Saucedo, A. *J. Chem. Soc., Faraday Trans. 1* **1979**, *75*, 736.

(29) Lewis, K. E.; Parfitt, G. D. *Trans. Faraday Soc.* **1966**, *62*, 204.

(30) Tanaka, K.; White, J. M. *J. Phys. Chem.* **1982**, *86*, 4708.

(31) Contescu, C.; Popa, V. T.; Schwarz, J. A. *J. Colloid Interface Sci.* **1996**, *180*, 149.

(32) Mul, G.; Zwijnenburg, A.; van der Linden, B.; Makkee, M.; Moulijn, J. A. *J. Catal.* **2001**, *201*, 128.

(33) Jackson, P.; Parfitt, G. D. *Trans. Faraday Soc.* **1971**, *67*, 2469.

(34) Groff, R. P.; Manogue, W. H. *J. Catal.* **1983**, *79*, 462.

(35) Busca, G. *Catal. Today* **1996**, *27*, 457.

(36) Coronado, J. M.; Kataoka, S.; Tejedo-Tejedor, I.; Anderson, M. A. *J. Catal.* **2003**, *219*, 219.

(37) Imanaka, T.; Okamoto, Y.; Teranishi, S. *Bull. Chem. Soc. Jpn.* **1972**, *45*, 3251.

(38) Gonzalezelipe, A. R.; Munuera, G.; Soria, J. *J. Chem. Soc., Faraday Trans. 1* **1979**, *75*, 748.

(39) Boehm, H. P. *Discuss. Faraday Soc.* **1971**, *52*, 264.

(40) Boonstra, A. H.; Mutsaers, C. A. H. A. *J. Phys. Chem.* **1975**, *79*, 1694.

(41) Muggli, D. S.; L., F. J. *J. Catal.* **2000**, *191*, 318.

(42) Lunsford, J. H. *Catal. Rev.* **1973**, *8*, 2251.

(43) Pichat, P.; Herrmann, J. M.; Courbon, H.; Disdier, J.; Mozzanega, M. N. *Can. J. Chem. Eng.* **1982**, *60*, 27.

(44) Sun, C. H.; Berg, J. C. *J. Chromatogr., A* **2002**, *969*, 59.

(45) Sekiya, T.; Ichimura, K.; Igarashi, M.; Kurita, S. *J. Phys. Chem. Solids* **2000**, *61*, 1237.

(46) Martra, G.; Coluccia, S.; Marchese, L.; Augugliaro, V.; Loddo, V.; Palmisano, L.; Schiavello, M. *Catal. Today* **1999**, *53*, 695.

(47) Nosaka, A. Y.; Fujiwara, T.; Yagi, H.; Akutsu, H.; Nosaka, Y. *Langmuir* **2003**, *19*, 1935.

(48) Lo, W. J.; Chung, Y. W.; Somorjai, G. A. *Surf. Sci.* **1978**, *71*, 199.